Sign of differential reflection and transmission in pump-probe spectroscopy of graphene on dielectric substrate

Chengmin Gao,[1] Xin Zhao,[2] Jun Yao,[1] Xiao-Qing Yan,[1,*] Xiang-Tian Kong,[1] Yongsheng Chen,[3] Zhi-Bo Liu,[1] and Jian-Guo Tian[1]

[1]*The Key Laboratory of Weak Light Nonlinear Photonics, Ministry of Education, Teda Applied Physics Institute and School of Physics, Nankai University, Tianjin 300457, China*
[2]*College of Science, Tianjin Polytechnic University, Tianjin 300387, China*
[3]*The Key Laboratory of Functional Polymer Materials and Center for Nanoscale Science & Technology, Institute of Polymer Chemistry, College of Chemistry, Nankai University, Tianjin 300071, China*
**Corresponding author: yanxq01@nankai.edu.cn*

Received December 24, 2014; revised February 9, 2015; accepted February 13, 2015; posted February 13, 2015 (Doc. ID 231254); published March 13, 2015

Pump-probe differential reflection and transmission spectroscopy is a very effective tool to study the nonequilibrium carrier dynamics of graphene. The reported sign of differential reflection from graphene is not explicitly explained and not consistent. Here, we study the differential reflection and transmission signals of graphene on a dielectric substrate. The results reveal the sign of differential reflection changes with the incident direction of the probe beam with respect to the substrate. The obtained theory can be applied to predict the differential signals of other two-dimensional materials placed on various dielectric substrates.

OCIS codes: (310.6870) Thin films, other properties; (190.4400) Nonlinear optics, materials; (160.4760) Optical properties; (190.7110) Ultrafast nonlinear optics.
http://dx.doi.org/10.1364/PRJ.3.0000A1

1. INTRODUCTION

Since a microscopic understanding of the nonequilibrium carrier dynamics of graphene is important for designing and implementing graphene-based high-speed optoelectronic devices [1–7], the relaxation of nonequilibrium carriers in the unique energy band has attracted significant attention in recent years [1,2,5,6,8–21]. These investigations have sparked novel contents in fundamental research, such as population invention [13] and collinear scattering [6]. At the same time, these works enrich the application of graphene in photonics [5,7,22].

Optical pump-probe differential reflection and transmission spectroscopy is a powerful tool to study the nonequilibrium carrier dynamics of graphene [23]. In the past years, various femtosecond pump-probe measurements were performed to probe the relaxation of photoexcited carriers in a variety of graphene films on different transparent dielectric substrates (such as quartz, SiC, CaF_2, and mica) [2,3,11,13–19]. Most of these works investigated the dynamics of the carriers by studying the temporal evolution of the differential signals [2,3,7,11,15,18]. Nevertheless, in addition to the temporal evolution of these differential signals, the sign of these signals is also related to interesting microscopic physics. It is known that the differential reflection and differential transmission signals come from the variation of the extinction coefficient $\Delta\kappa$ (or optical conductivity $\Delta\sigma$) after the optical pumping [8,12,23]. This $\Delta\kappa$ can be negative due to the bleaching of the interband transitions by Pauli blocking (i.e., $\Delta\kappa < 0$ and $\Delta\sigma < 0$) [2,12,15,17] or be positive due to the intraband absorption, the increase of the Hartree–Fock self-energy, and the variation of the scattering (i.e., $\Delta\kappa > 0$ and $\Delta\sigma > 0$) [8,12,23,24]. To identify which mechanism is dominant (i.e., the sign of $\Delta\kappa$) from differential signals of graphene on dielectric substrate, a specific relationship between the experimental obtained differential signals and $\Delta\kappa$ is needed. However, this relationship has not been explored so far, despite the large number of microscopic studies on $\Delta\kappa$ (or $\Delta\sigma$) [8,23,25]. In addition, the sign of differential signals reported in literature is not consistent [10,15]. To understand these works and study carrier dynamics of graphene, we need to further theoretically bridge the universal relationship between the differential signals and $\Delta\kappa$ for graphene on a substrate.

The optical absorbance of monolayer graphene is ~2.3% [26]; as a result, it is hard to precisely judge which side of the transparent substrate the monolayer graphene is on, using eyes and ordinary optical microscopes. In the experiment, the possibility of confusing the two sides could not be absolutely avoided [Fig. 1(a)]. It is interesting to know the influence of confusing the two sides on the differential signals. Thus, knowing the relationship between these differential signals and the pump-induced $\Delta\kappa$ under different incident directions of the probe beam is helpful [i.e., *Case 1*: from graphene to substrate, and *Case 2*: from substrate to graphene, Fig. 1(a)].

In this paper, we calculate the time-resolved pump-probe differential signals of graphene on a dielectric substrate for the two incident directions of probe beam. The presented theory could explain the sign of differential signals resulting from optical pump-induced $\Delta\kappa$ of graphene. It shows that if we

turn the graphene sample around with respect to the incident direction of the probe beam the sign of differential reflection is reversed, but the sign of differential transmission remains unchanged. Our results are helpful for ultrafast carrier dynamics study of two-dimensional (2D) materials placed on a dielectric substrate.

2. THEORY

It is known that the differential reflection and differential transmission signals are direct consequences of pump-induced $\Delta\kappa$ (or $\Delta\sigma$) of graphene [8,12,23]. To calculate the differential signals measured by ultrashort laser pulses, we first calculate the reflectance R and transmittance T of graphene on substrate with and without optical pumping. Based on the R and T of ultrashort pulses, we could establish the relationship between differential signals and $\Delta\kappa$.

Figure 1(a) shows the incidence of the probe beam into the graphene sample for the two cases. For both cases, the middle graphene–substrate layers and the two semi-infinite air layers compose a four-layer structure (*Layer4*) [27,28]. Clearly, the optical response of this structure is the result of collective action of a three-layer structure (*Layer3*, i.e., air–graphene–substrate) and a two-layer structure (*Layer2*, i.e., air–substrate) [29]. To analyze the R and T of ultrashort pulses from this structure, we need to know in advance the R and T of a plane wave in the structures *Layer2* and *Layer3*. In fact, all the two structures could be unified as a multilayer structure (*Layern*), as shown in Fig. 1(b). For simplicity, we will first analyze the R and T of a plane wave for the structure *Layern* based on Maxwell's equations solving boundary conditions; then we obtain the R and T for *Layer2* and *Layer3* from these of *Layern*. Following, we calculate the R and T of ultrashort pulses from graphene on substrate (including both cases). Since the incident beam used in most graphene pump-probe experiments is at optical frequency, and the graphene is exposed in an environment free from external magnetic fields [8,9,12,15,17–19], graphene is modeled as an

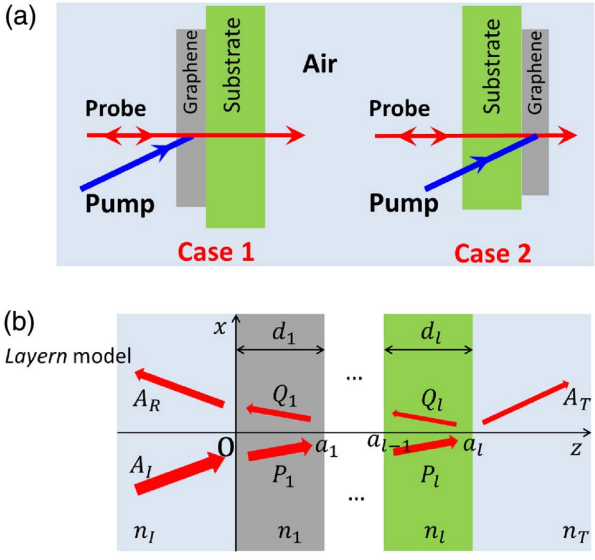

Fig. 1. (a) Scheme of pump-probe measurement in graphene placed on dielectric substrate; opposite incident direction of probe beam is depicted. *Case 1*: from graphene to substrate; *Case 2*: from substrate to graphene. (b) Generalized multilayer structure model.

isotropic insulating film with finite thickness, as done by Weber *et al.*, Bruna *et al.*, Nelson *et al.*, and Ye *et al.* [27,30–32].

A. Multilayer Structure Theory

The modeled multilayer structure is shown in Fig. 1(b). A plane wave is assumed incident into this structure. The plane of incidence is in the x, z plane, and all the boundaries are perpendicular to the z direction. This structure consists of l ($l \geq 0$) slabs sandwiched between two semi-infinite spaces (i.e., incident and exit spaces). The boundaries are given by $z = a_0, a_1, \ldots, a_l$ with $a_0 = 0$. The refractive indices of incident and exit spaces are given by $n_I = \sqrt{\varepsilon_I \mu_I}$ and $n_T = \sqrt{\varepsilon_T \mu_T}$, respectively. The thickness and refractive index of the ith slab are given by $d_i = a_i - a_{i-1}$ and $n_i = \sqrt{\varepsilon_i \mu_i} (i = 1, 2, \ldots, l)$, respectively. Here, ε_I, ε_T, ε_i and μ_I, μ_T, μ_i are the corresponding relative permittivity and relative permeability. For the graphene, the complex refractive index (i.e., optical constant) is $n_g = n_0 + i\kappa$ [30,33]; n_0 and κ are the refractive index and the extinction coefficient of graphene, respectively. As listed in Fig. 1(b), A_I, A_R, A_T, P_i, and $Q_i (i = 1, 2, \ldots, l)$ are the amplitude of the light field in different layers.

The electric field direction of the incident beam is assumed to be along the y axis, that is, E_x, E_z, $H_y = 0$ and $\partial/\partial_y = 0$. Therefore, the Maxwell's equations can be deduced to be (time envelope $e^{-i\omega t}$ is assumed) [29]

$$\frac{\partial H_x}{\partial z} - \frac{\partial H_z}{\partial x} + i\omega\varepsilon E_y = 0, \tag{1}$$

$$\frac{\partial E_y}{\partial z} + i\omega\mu H_x = 0, \tag{2}$$

$$\frac{\partial E_y}{\partial x} - i\omega\mu H_z = 0. \tag{3}$$

The waves in each layer can be represented as superpositions of positive- (along $+z$) and negative (along $-z$)-going secondary waves. Thus, E_y is written as follows:

$$E_y = (A_I e^{ik_{Iz}z} + A_R e^{-ik_{Iz}z}) e^{ik_x x} \quad \text{for } z \leq a_0 = 0, \tag{4}$$

$$E_y = (P_i e^{ik_{iz}(z-a_{i-1})} + Q_i e^{-ik_{iz}(z-a_i)}) e^{ik_x x} \quad \text{for } a_{i-1} \leq z \leq a_i (i = 1, 2, \ldots, l), \tag{5}$$

$$E_y = A_T e^{ik_{Tz}(z-a_l)} e^{ik_x x} \quad \text{for } z \geq a_l. \tag{6}$$

Here $k_{Iz} = \sqrt{n_I^2 k_0^2 - k_x^2}$, $k_{iz} = \sqrt{n_i^2 k_0^2 - k_x^2} (i = 1, 2, \ldots, l)$, $k_{Tz} = \sqrt{n_T^2 k_0^2 - k_x^2}$, and $k_x = n_I k_0 \sin\theta_I$, where θ_I is incident angle of the probe beam, $k_0 = 2\pi/\lambda_0$ is the wave vector in vacuum, and λ_0 is the wavelength of the probe beam in vacuum.

Based on Eqs. (1) through (6), the magnetic field components in each layer are given as

$$H_x = \frac{1}{-i\omega\mu} \frac{\partial E_y}{\partial z}, \tag{7}$$

$$H_z = \frac{k_x}{\omega\mu} E_y. \tag{8}$$

According to the continuities for E_y and H_x at the boundary, we can obtain:

at $z = a_0 = 0$,

$$\begin{cases} A_I + A_R = (P_1 + Q_1 e^{ik_{1z}d_1}) \\ \frac{k_{Iz}}{\mu_I}(A_I - A_R) = \frac{k_{1z}}{\mu_1}(P_1 - Q_1 e^{ik_{1z}d_1}) \end{cases}, \tag{9}$$

at $z = a_i (i = 1, 2, \ldots, l-1)$,

$$\begin{cases} P_i e^{ik_{iz}d_i} + Q_i = P_{i+1} e^{ik_{i+1,z}d_{i+1}} + Q_{i+1} \\ \frac{k_{iz}}{\mu_i}(P_i e^{ik_{iz}d_i} - Q_i) = \frac{k_{i+1,z}}{\mu_{i+1}}(P_{i+1} e^{ik_{i+1,z}d_{i+1}} - Q_{i+1}) \end{cases}, \tag{10}$$

at $z = a_l$,

$$\begin{cases} P_l e^{ik_{lz}d_l} + Q_l = A_T \\ \frac{k_{lz}}{\mu_l}(P_l e^{ik_{lz}d_l} - Q_l) = \frac{k_{Tz}}{\mu_T} A_T \end{cases}. \tag{11}$$

According to Eqs. (9) through (11), the relations between the amplitude coefficients are given by

$$\begin{bmatrix} A_I \\ A_R \end{bmatrix} = m_0 \begin{bmatrix} P_1 \\ Q_1 \end{bmatrix}, \tag{12}$$

$$\begin{bmatrix} P_i \\ Q_i \end{bmatrix} = m_i \begin{bmatrix} P_{i+1} \\ Q_{i+1} \end{bmatrix}, \tag{13}$$

$$\begin{bmatrix} P_l \\ Q_l \end{bmatrix} = m_l A_T, \tag{14}$$

where

$$m_0 = \frac{1}{2}\begin{bmatrix} 1 + K_{1I}\Gamma_{I1} & (1 - K_{1I}\Gamma_{I1})e^{i\beta_1} \\ 1 - K_{1I}\Gamma_{I1} & (1 + K_{1I}\Gamma_{I1})e^{i\beta_1} \end{bmatrix}, \tag{15}$$

$$m_i = \frac{1}{2}\begin{bmatrix} (1 + K_{i+1,i}\Gamma_{i,i+1})e^{-i\beta_i} & (1 - K_{i+1,i}\Gamma_{i,i+1})e^{i\beta_{i+1}}e^{-i\beta_i} \\ 1 - K_{i+1,i}\Gamma_{i,i+1} & (1 + K_{i+1,i}\Gamma_{i,i+1})e^{i\beta_{i+1}} \end{bmatrix}. \tag{16}$$

$$m_l = \frac{1}{2}\begin{bmatrix} (1 + K_{Tl}\Gamma_{lT})e^{-i\beta_l} \\ 1 - K_{Tl}\Gamma_{lT} \end{bmatrix}. \tag{17}$$

Here $K_{1I} = \frac{\sqrt{n_1^2 - n_I^2 \sin^2\theta_I}}{n_I \cos\theta_I}$, $K_{i+1,i} = \frac{\sqrt{n_{i+1}^2 - n_I^2 \sin^2\theta_I}}{\sqrt{n_i^2 - n_I^2 \sin^2\theta_I}}$, $K_{Tl} = \frac{\sqrt{n_T^2 - n_I^2 \sin^2\theta_I}}{\sqrt{n_l^2 - n_I^2 \sin^2\theta_I}}$, $\Gamma_{I1} = \frac{\mu_I}{\mu_1}$, $\Gamma_{i,i+1} = \frac{\mu_i}{\mu_{i+1}}$, $\Gamma_{lT} = \frac{\mu_l}{\mu_T}$, $\beta_i = \sqrt{n_i^2 - n_I^2 \sin^2\theta_I} k_0 d_i$, $\beta_l = \sqrt{n_l^2 - n_I^2 \sin^2\theta_I} k_0 d_l$, and $i = 1, 2, \ldots, (l-1)$.

The amplitudes of the incident beam, reflected beam, and transmitted beam are relationed as

$$\begin{bmatrix} A_I \\ A_R \end{bmatrix} = M A_T, \tag{18}$$

where M is a 2×1 matrix and is defined as

$$M = \begin{bmatrix} M_1 \\ M_2 \end{bmatrix} = \prod_{i=0}^{l} m_i. \tag{19}$$

Thus, the complex electric field amplitude of the reflected and transmitted beams is related to that of the incident beam by $A_R = \frac{M_2}{M_1} A_I = r A_I$ and $A_T = \frac{1}{M_1} A_I = t A_I$. r and t denote the amplitude reflection and transmission coefficient, respectively. The R and T are given by

$$R = \left|\frac{A_R}{A_I}\right|^2 = |r|^2, \tag{20}$$

$$T = \frac{\mu_I}{\mu_T}\frac{\Re(k_{Tz})}{k_{Iz}}\left|\frac{A_T}{A_I}\right|^2 = \frac{\mu_I}{\mu_T}\frac{\Re(k_{Tz})}{k_{Iz}}|t|^2. \tag{21}$$

In the following, we calculate the R and T of a normally incident beam ($\theta_I = 0$) for *Layer2* and *Layer3* from the above equations (since the probe beam is usually normally incident into graphene [8,9,11,15], the incident angle of the probe beam is set to be zero). To denote the incident direction of light in the equations, we will write the refractive index of each layer in the order from incident space to exit space.

B. Layer2

For the structure *Layer2*, the reflectance and transmittance of a normally incident beam can be reduced as

$$R_2(n_I, n_T) = |r|^2 = \left|\frac{n_I - n_T}{n_I + n_T}\right|^2, \tag{22}$$

$$T_2(n_I, n_T) = \frac{n_T}{n_I}|t|^2 = \frac{n_T}{n_I}\left|\frac{2n_I}{n_I + n_T}\right|^2. \tag{23}$$

These results are known as the Fresnel formula [29].

C. Layer3

For the structure *Layer3* ($l = 1$), the R and T of a normally incident beam simplify to

$$R_3(n_I, n_1, n_T) = |r|^2 = \left|\frac{r_{I1} + r_{1T}e^{i2\beta_1}}{1 + r_{I1}r_{1T}e^{i2\beta_1}}\right|^2, \tag{24}$$

$$T_3(n_I, n_1, n_T) = \frac{n_T}{n_I}|t|^2 = \frac{n_T}{n_I}\left|\frac{t_{I1}t_{1T}e^{i\beta_1}}{1 + r_{I1}r_{1T}e^{i2\beta_1}}\right|^2. \tag{25}$$

Here $r_{I1} = \frac{n_I - n_1}{n_I + n_1}$, $r_{1T} = \frac{n_1 - n_T}{n_1 + n_T}$, $t_{I1} = \frac{2n_I}{n_I + n_1}$, $t_{1T} = \frac{2n_1}{n_1 + n_T}$, and $\beta_1 = n_1 k_0 d_1$. Clearly, the reflectance and transmittance are functions of the extinction coefficient of each layer.

For the structure *Layern*, each middle layer (i.e., slab $n_1 \ldots n_l$) could be regarded as a Fabry–Perot cavity [34]. As we know, the incident beam will be split into infinite reflected and transmitted waves of decreasing intensities due to multiple

reflections in each middle layer. Clearly, the reflection and transmission of structure *Layern* is the collective contribution of these reflected and transmitted waves, resulting from multiple reflections in each layer (Fig. 2) [34]. The above calculation is performed on the assumption that these reflected and transmitted waves are temporally coherent, which is of course applicable to a plane wave. However, for incidence of a laser pulse, the multiple reflections will ultimately lead to the creation of a number of secondary reflected and transmitted subpulses of decreasing intensities. These reflected/transmitted subpulses are separated in the reflection/transmission direction (Fig. 2). The analysis presented above may no longer hold in the case of ultrashort pulses where the temporal coherence would need to be taken into account. Therefore, the R and T presented above are valid for continuous light and pulses with a coherence length much longer than the thickness of the middle layers (for this case, the separation between two successive reflected/transmitted subpulses is very short as compared with the coherence length of pulses) [35]. Since there is no multiple reflection process for the structure *Layer2*, Eqs. (22) and (23) are available for ultrashort pulses besides continuous light.

D. R and T of Ultrashort Laser Pulse from Graphene on Substrate

In the graphene pump-probe experiment, the thickness of the graphene film is generally smaller than 3.4 nm (i.e., 10-layer graphene), and the thickness of the substrate is in the order of 1 mm; the pulse width τ_{FWHM} is generally less than 400 fs (coherence length is less than 0.29 mm) [2–5,8,12,15–17]. It takes less than 0.068 fs for pulses passing one round trip in the graphene layer, corresponding to an optical path length of 6.8 nm. However, for one round trip in the substrate (optical path length is 2 mm), it takes about 10 ps. This means these reflected/transmitted ultrashort subpulses from the graphene layer are temporally coherent, but these reflected/transmitted ultrashort subpulses from the substrate are temporally noncoherent (i.e., they are separated in the reflection/transmission direction; see Fig. 2). Therefore, the R and T of ultrashort pulses from graphene on substrate could not be obtained as *Layer4* from the results of *Layern*.

As shown in Fig. 2, the structure of graphene on substrate (air–graphene–substrate–air) could be regarded as a combination of a *Layer3* structure (i.e., air–graphene–substrate) and a

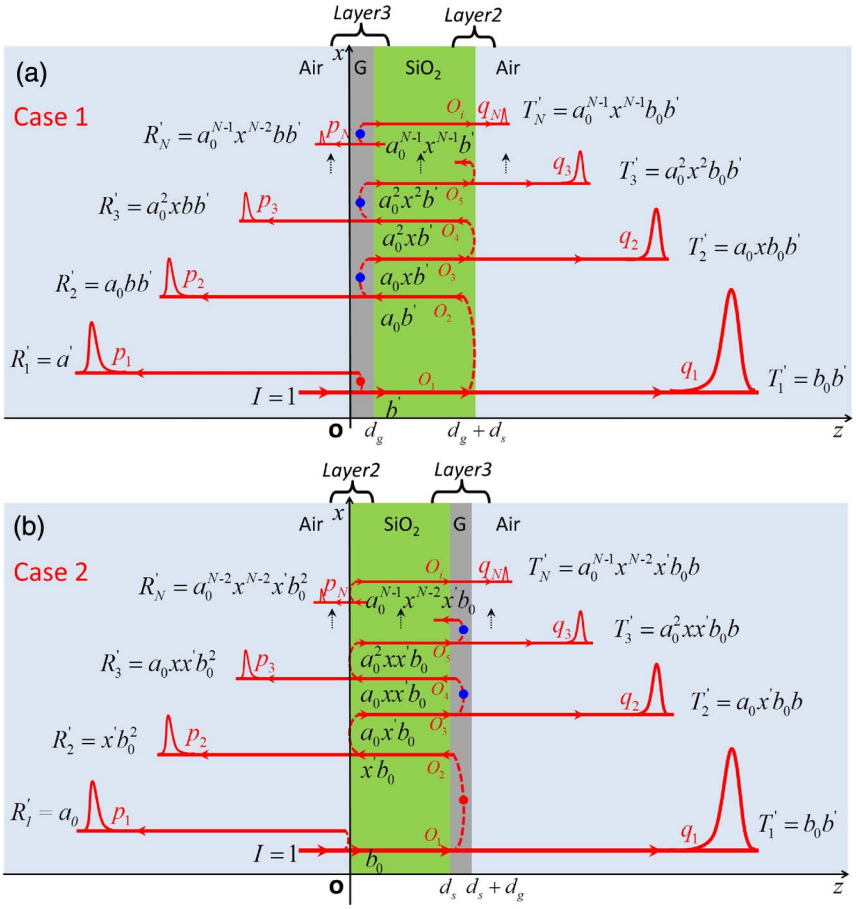

Fig. 2. Multiple reflections and calculation of the reflectance as well as transmittance when an ultrashort probe pulse is normally incident into optically excited graphene on substrate. In order to guide the eyes, the reflected and transmitted subpulses are artificially shifted upward. The red dot is used to indicate that the extinction coefficient of graphene is changed by optical pumping, and the blue dots indicate that the pump-induced $\Delta\kappa$ nearly vanishes (i.e., $\Delta\kappa \approx 0$) due to carrier relaxation. The incident beam is assumed to have an intensity of one; the intensity ratio of each reflected/transmitted subpulse to the incident pulse is corresponding marked. For simplicity, substitutions are used in the figure. For *Layer2* $a_0 = R_2(n_a, n_s) = R_2(n_s, n_a)$, $b_0 = T_2(n_a, n_s) = T_2(n_s, n_a)$; for *Layer3* without extinction coefficient change ($\Delta\kappa = 0$), $a = R_3(n_a, n_g, n_s)$, $x = R_3(n_s, n_g, n_a)$, $b = T_3(n_a, n_g, n_s) = T_3(n_s, n_g, n_a)$; for *Layer3* with extinction coefficient change, $a' = R_3(n_a, n_{g,\mathrm{pump}}, n_s)$, $x' = R_3(n_s, n_{g,\mathrm{pump}}, n_a)$, and $b' = T_3(n_a, n_{g,\mathrm{pump}}, n_s) = T_3(n_s, n_{g,\mathrm{pump}}, n_a)$. If there is no optical pumping in graphene, the extinction coefficient of graphene is $n_g = n_0 + i\kappa$ for all these multiple reflections, and the intensity ratio of each reflected/transmitted subpulse should change.

Layer2 structure (i.e., substrate–air). On the other hand, since these reflected/transmitted subpulses resulting from multiple reflections in the graphene layer are coherent, we can regard the structure of air–graphene–substrate as an integrated *Layer3* structure (i.e., an interface with two semi-infinite spaces). Also, Eqs. (24) and (25) could be applied to calculate the R and T of the graphene layer at the interface with the substrate (i.e., air–graphene–substrate, with $n_1 = n_g = n_0 + i\kappa$). Thus, we need only consider the influence of multiple reflections in substrate for both cases. As illustrated in Fig. 2, we present the reflected and transmitted subpulses, as well as multiple reflections in substrate for both cases.

The total reflected/transmitted intensity from graphene on substrate is the sum of all individual reflected/transmitted subpulses' intensities, as these reflected/transmitted subpulses are temporally noncoherent in their propagation direction. Therefore, the reflectance/transmittance of both cases could be calculated by integrating the intensity ratios of the reflected/transmitted subpulse to the incident pulse (Fig. 2). By integrating, the R and T of an ultrashort laser pulse from graphene on substrate (no optical pumping) could be written as follows:

For *Case 1*,

$$R_4(n_a, n_g, n_s, n_a) = R_3(n_a, n_g, n_s) + \frac{R_2(n_a, n_s)T_3^2(n_a, n_g, n_s)}{1 - R_2(n_a, n_s)R_3(n_s, n_g, n_a)}, \quad (26)$$

$$T_4(n_a, n_g, n_s, n_a) = \frac{T_2(n_a, n_s)T_3(n_a, n_g, n_s)}{1 - R_2(n_a, n_s)R_3(n_s, n_g, n_a)}. \quad (27)$$

For *Case 2*,

$$R_4(n_a, n_s, n_g, n_a) = R_2(n_a, n_s) + \frac{R_3(n_s, n_g, n_a)T_2^2(n_a, n_s)}{1 - R_2(n_a, n_s)R_3(n_s, n_g, n_a)}, \quad (28)$$

$$T_4(n_a, n_s, n_g, n_a) = \frac{T_2(n_a, n_s)T_3(n_a, n_g, n_s)}{1 - R_2(n_a, n_s)R_3(n_s, n_g, n_a)}, \quad (29)$$

where n_a and n_s are the refractive index of air and substrate, respectively. $n_g = n_0 + i\kappa$ is the optical constant of graphene. These equations are calculated based on the assumption of no refractive index change during incidence and multiple reflection processes. They are applied to the case of no optical pumping.

E. Time-resolved Pump-Probe Differential Signals

In the graphene pump-probe experiment, the extinction coefficient of graphene changes after optical pumping, and the pump-induced $\Delta\kappa$ leads to the change in reflectance and transmittance. The magnitude of $\Delta\kappa$ is governed by the population of nonequilibrium carriers at optically probed state and decays with the carrier relaxation. It is reported that the carrier population at optically probed state decreases with relaxation time t in a biexponential function. Thus, we could describe the decay of extinction coefficient change as $\Delta\kappa(t) = \Delta\kappa_0(e^{-t/\tau_1} + \alpha e^{-t/\tau_2})/2$, where $\tau_1 = 110 \pm 40$ fs and $\tau_2 = 900 \pm 200$ fs [3,4], and parameter α describes the weight of the two relaxation pathways [8,10,18]. As discussed above, the time for one round trip in substrate is about 10 ps, during which the nonequilibrium carriers have undergone sufficient relaxation. Correspondingly, $\Delta\kappa$ decays to nearly zero. (The intensity of the multiply reflected pump subpulse is much lower than that of the pump pulse, and the propagation direction of the subpulse from the pump pulse is generally not identical to that of subpulse from the probe pulse. The optical excitation induced by the subpulse from the pump pulse could be ignored). Therefore, when a probe pulse is incident into optically excited graphene on substrate with optical pumping delayed by t_{delay}, the extinction coefficient change $\Delta\kappa(t_{\text{delay}})$ should be taken into account for the first incidence of the probe pulse into the graphene layer (as shown by the red dot in Fig. 2); for the successive multiple reflections, the extinction coefficient change is negligible (i.e., $\Delta\kappa \approx 0$, as shown by the blue dot in Fig. 2). As shown in Fig. 2(b), the differential reflection signal of *Case 2* is generated by the first reflection at the *Layer3* structure (reversed, i.e., substrate–graphene–air). For the convenience of the following presentation, we will refer to the reflections of $O_3 \ldots O_i$ at the substrate interfaces as multiple reflections for *Case 2* [Fig. 2(b)] and refer to the reflections of $O_1 \ldots O_i$ as multiple reflections for *Case 1* [Fig. 2(a)].

With this picture of the decay of $\Delta\kappa(t)$, the intensity ratio of each reflected/transmitted subpulse to the incident pulse could be obtained (Fig. 2). The reflectance and transmittance of the probe pulse from optically excited graphene on substrate could be written as follows:

For *Case 1*,

$$R_4(n_a, n_{g,\text{pump}}, n_s, n_a) = R_3(n_a, n_{g,\text{pump}}, n_s) + \frac{R_2(n_a, n_s)T_3(n_a, n_g, n_s)T_3(n_a, n_{g,\text{pump}}, n_s)}{1 - R_2(n_a, n_s)R_3(n_s, n_g, n_a)}, \quad (30)$$

$$T_4(n_a, n_{g,\text{pump}}, n_s, n_a) = \frac{T_2(n_a, n_s)T_3(n_a, n_{g,\text{pump}}, n_s)}{1 - R_2(n_a, n_s)R_3(n_s, n_g, n_a)}. \quad (31)$$

For *Case 2*

$$R_4(n_a, n_s, n_{g,\text{pump}}, n_a) = R_2(n_a, n_s) + \frac{R_3(n_s, n_{g,\text{pump}}, n_a)T_2^2(n_a, n_s)}{1 - R_2(n_a, n_s)R_3(n_s, n_g, n_a)}, \quad (32)$$

$$T_4(n_a, n_s, n_{g,\text{pump}}, n_a) = T_2(n_a, n_s) \times \left[T_3(n_a, n_{g,\text{pump}}, n_s) + \frac{R_2(n_a, n_s)R_3(n_s, n_{g,\text{pump}}, n_a)T_3(n_a, n_g, n_s)}{1 - R_2(n_a, n_s)R_3(n_s, n_g, n_a)} \right], \quad (33)$$

where $n_{g,\text{pump}} = n_0 + (\kappa + \Delta\kappa(t_{\text{delay}}))i$ is the complex refractive index of optically excited graphene when the probe pulse is incident into the graphene.

According to the R and T with and without optical pumping, the optical pump-induced differential reflection and differential transmission are given as follows:

For *Case 1*,

$$\Delta R(t_{\text{delay}})/R = R_4(n_a, n_{g,\text{pump}}, n_s, n_a)/R_4(n_a, n_g, n_s, n_a) - 1, \tag{34}$$

$$\Delta T(t_{\text{delay}})/T = T_4(n_a, n_{g,\text{pump}}, n_s, n_a)/T_4(n_a, n_g, n_s, n_a) - 1. \tag{35}$$

For *Case 2*

$$\Delta R(t_{\text{delay}})/R = R_4(n_a, n_s, n_{g,\text{pump}}, n_a)/R_4(n_a, n_s, n_g, n_a) - 1, \tag{36}$$

$$\Delta T(t_{\text{delay}})/T = T_4(n_a, n_s, n_{g,\text{pump}}, n_a)/T_4(n_a, n_s, n_g, n_a) - 1. \tag{37}$$

With carrier relaxation, $\Delta\kappa(t_{\text{dealy}})$ decreases with decay time t_{delay}. As a result, the relative values of $\Delta R(t_{\text{delay}})/R$ and $\Delta T(t_{\text{delay}})/T$ decay with carrier relaxation. The time-resolved pump-probe differential signals are proportional to the convolution of $\Delta R(t)/R$, $\Delta T(t)/T$, and the Gaussian intensity distribution of the probe pulse as

$$(\Delta R(t)/R)_{p-p} = \frac{2\sqrt{\ln 2}}{\sqrt{\pi}\tau_{\text{FWHM}}}\left[\frac{\Delta R(t)}{R} * f(t)\right], \tag{38}$$

$$(\Delta T(t)/T)_{p-p} = \frac{2\sqrt{\ln 2}}{\sqrt{\pi}\tau_{\text{FWHM}}}\left[\frac{\Delta T(t)}{T} * f(t)\right], \tag{39}$$

where $f(t) = \exp(-(\sqrt{2\ln 2}t/\tau_{\text{FWHM}})^2)$ is a typical Gaussian function.

3. RESULTS AND DISCUSSION

A. Dependence of $\Delta R/R$ and $\Delta T/T$ on $\Delta\kappa$

To study the sign of time-resolved pump-probe differential signals, we first look into the dependence of the change in reflection and transmission on $\Delta\kappa$ from Eqs. (34) through (37). Here, we take monolayer graphene on a 1 mm thick quartz ($n_s = 1.543$) as an example. The wavelength of the probe pulse is assumed to be the widely used 800 nm, and the optical constant of graphene at 800 nm is $n_g = 3.0 + 1.4523i$ [30].

As shown by solid lines in Fig. 3, $\Delta T/T$ is inversely proportional to the $\Delta\kappa$ for the two cases [30]. Thus, the sign of $\Delta T/T$ is opposite to the sign of $\Delta\kappa$ for both cases. However, $\Delta R/R$ is proportional to $\Delta\kappa$ for *Case 1* and inversely proportional to $\Delta\kappa$ for *Case 2*. Corresponding, the sign of $\Delta R/R$ is identical to that of $\Delta\kappa$ for *Case 1* and opposite to that of $\Delta\kappa$ for *Case 2*. The opposite sign of $\Delta R/R$ for both cases stems from the structure *Layer3*, as the contribution of $\Delta\kappa$ to differential signals occurs in the structure *Layer3* (Fig. 2). Detailed analysis on the structure *Layer3* shows that the reflection change caused by $\Delta\kappa$ is related to the refractive index distribution of incident and exit spaces.

As a comparison, the dependence of $\Delta R/R$ and $\Delta T/T$ on $\Delta\kappa/\kappa$ was calculated under the assumption of no $\Delta\kappa$ relaxation in multiple reflections process. For *Case 1*, the multiple reflections alter the magnitude of $\Delta R/R$ but do not alter $\Delta T/T$ (dashed lines in Fig. 3). For *Case 2*, there is no visible influence of multiple reflections on these differential signals. Therefore, when the decay time of $\Delta\kappa$ is much longer than the time for one round trip in substrate, the contribution of multiple reflections to $\Delta R/R$ of *Case 1* should be considered, but this contribution does not change the sign of $\Delta R/R$. However, the contribution of multiple reflections to the $\Delta T/T$ of *Case 1*, $\Delta R/R$, and $\Delta T/T$ of *Case 2* is negligible (Fig. 3).

B. Time-resolved Pump-Probe Differential Reflection and Transmission

Based on Eqs. (38) and (39), we could calculate the time-resolved pump-probe differential signals for the two cases and compare the theoretical results with experiment. As shown in Fig. 3, the $\Delta R/R$ and $\Delta T/T$ monotonously change with $\Delta\kappa$ for both cases. This indicates the differential signals induced by intraband absorption of hot carriers ($\Delta\kappa > 0$) is opposite to those caused by Pauling blocking ($\Delta\kappa < 0$). For simplicity and matching with our experiment, we will only discuss time-resolved pump-probe differential signals caused by Pauling blocking here.

The calculated time-resolved pump-probe differential signals are shown in Fig. 4 for both cases. The $(\Delta T(t)/T)_{p-p}$ is positive and nearly identical for both cases. The $(\Delta R(t)/R)_{p-p}$ is negative for *Case 1* and positive for *Case 2*. Also, the magnitude of $(\Delta R(t)/R)_{p-p}$ is different for the two

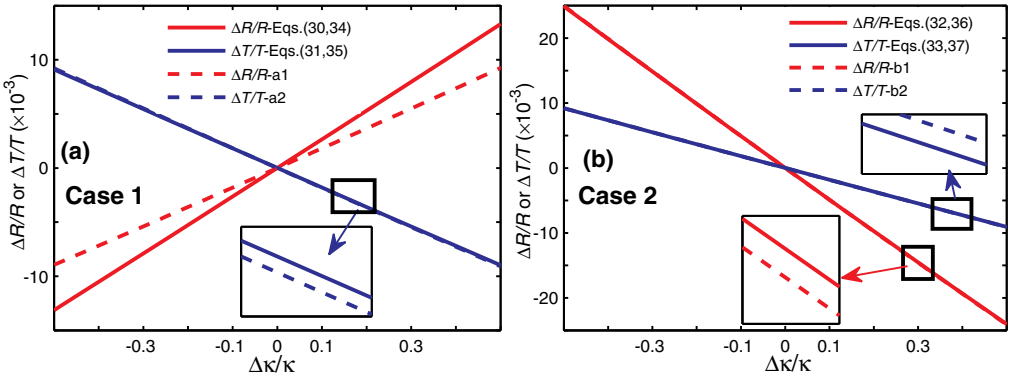

Fig. 3. $\Delta R/R$ and $\Delta T/T$ of graphene on quartz versus $\Delta\kappa/\kappa$ for (a) *Case 1* and (b) *Case 2*. The dashed lines are calculated based on the assumption that the $\Delta\kappa$ does not relax with time (i.e., identical $\Delta\kappa$ for these multiple reflections at the interface with graphene). Inserts: zoomed-in view of the overlapped lines.

cases. Thus, if we change the incident direction of the probe beam, the sign of $(\Delta R(t)/R)_{p-p}$ will be reversed, but $(\Delta T(t)/T)_{p-p}$ remains positive. Based on the relationship between the sign of $(\Delta R(t)/R)_{p-p}$ and the incident direction, the substrate facet with graphene layer could be determined by pump-probe measurement. Although the magnitude and sign of these differential signals are different, the normalized differential signals are identical (not shown here). This means that there is no influence of the incident direction on the relaxation time of these differential signals.

To confirm the sign of differential signals predicted by theory, the 800 nm degenerate pump-probe measurement was performed on a chemical vapor deposited grown monolayer graphene placed on a 1 mm thick quartz; the width (FWHM) of 800 nm pulses was 350 ± 30 fs. It is known that the nonequilibrium carriers at this optically probed state (0.775 eV) block the corresponding interband transitions and cause a decrease in κ and σ due to Pauli blocking [3,11,17]. The quartz face with graphene film was marked to avoid confusing the incident direction. As Fig. 4 shows, the sign of measured differential signals is in good agreement with the theoretical result and consistent with former reports [Figs. 4(a) and 4(b)] [11,12,15,18].

For the suspended graphene, the reflectance and transmittance could be directly obtained from those of structure *Layer3*. So, $\Delta R(t_{\text{delay}})/R = R_3(n_a, n_{g,\text{pump}}, n_a)/R_3(n_a, n_g, n_a) - 1$, $\Delta T(t_{\text{delay}})/T = T_3(n_a, n_{g,\text{pump}}, n_a)/T_3(n_a, n_g, n_a) - 1$. The reported negative $(\Delta R(t)/R)_{p-p}$ of suspended graphene could be explained with these equations (not shown here) [12].

In the theory analysis, the graphene layer was assumed as a very thin dielectric layer. Therefore, the present theory could be applied for other 2D materials [36–38], and the studied 2D material could be multilayer. To make sure the reflected and transmitted subpulses are temporally coherent, the layer number of the sample should be not very large. The carrier relaxation of these 2D materials may be not fast, as compared with the time for one round trip in substrate [36–38]. For this case, $\Delta\kappa$ is not negligible in the initial multiple reflection process. As shown above, the influence of initial multiple reflections on $\Delta R/R$ should be taken into account for *Case 1*, such as $R'_2 = a_0(b')^2$ for subpulse p_2 and $T'_2 = a_0 x' b_0 b'$ for subpulse q_2 in Fig. 2(a). However, in the calculation of $\Delta T/T$, the contribution of multiple reflections could be ignored. For *Case 2*, the influence of multiple reflections on both differential signals is negligible, no matter the decay time of $\Delta\kappa$.

As shown above, $(\Delta T(t)/T)_{p-p}$ does not change with structure and incident direction. Therefore, to study the carrier relaxation of these 2D materials, it is better to use $(\Delta T(t)/T)_{p-p}$ instead of $(\Delta R(t)/R)_{p-p}$ since the wrong conclusion resulting from confusing the incident direction could be avoided. From the view point of influence of multiple reflections on the differential signals, it is also suggested to use $(\Delta T(t)/T)_{p-p}$.

In our analysis, the probe beam is normally incident into the sample. If the probe beam is obliquely incident into the sample, the reflected and transmitted subpulses from the graphene layer are temporally coherent. We could still regard the graphene at the interface as a *Layer3* structure. The R_3 and T_3 of an obliquely incident beam could be numerically calculated from Eqs. (19)–(21). Similar to the case of normal incidence, the total reflected/transmitted intensity is the sum of all individual reflected/transmitted subpulses' intensities. The calculation indicates that the sign of differential signals does not vary if the probe pulses are incident into the sample with a small angle.

In a degenerate pump-probe experiment, the pump-induced $\Delta\kappa$ near zero delay time is dependent on the relative orientation of pump polarization and probe polarization [19]. $\Delta\kappa$ is

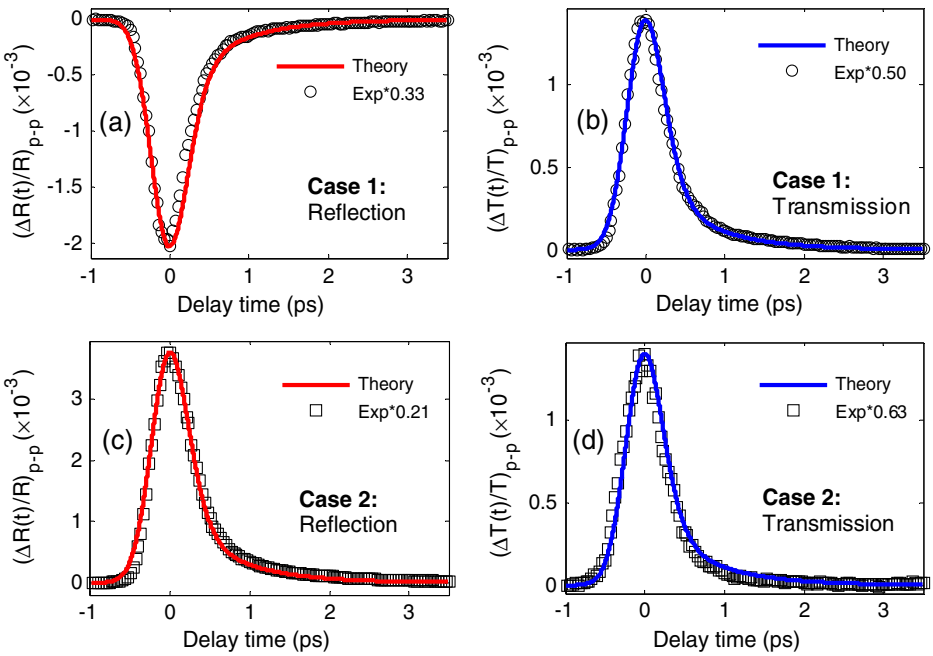

Fig. 4. Time-resolved pump-probe differential signals versus delay time for both cases. Solid lines denote the theoretical results (Δk_0 was randomly set to be –0.32), while circles and squares denote the experimental results. The experiment data is scaled to match the theoretical curves. Owing to the sign of differential signals is concerned here, the pump fluence in each measurement is randomly selected. The pump fluence is about (a) 1.2, (b) 1.9, (c) 2.9, and (d) 1.72 mJ/cm^2.

the maximum/minimum for the probe beam with polarization parallel/perpendicular to the pump polarization. Since the differential signals are functions of $\Delta\kappa$ for both cases, the magnitude of differential signals near zero delay time should be polarization dependent in degenerate pump-probe measurement, but the sign does not change with polarizations of beams.

4. SUMMARY

We provided a generic theoretical framework for predicting pump-induced differential reflection and differential transmission signals of thin film on top of a dielectric substrate. The theory could well explain the sign of time-resolved pump-probe differential signals of graphene on substrate. The sign of differential reflection depends on the incident direction of the probe beam with respect to the substrate, but the sign of differential transmission remains unchanged when the sample is turned round. This is useful for analyzing the interaction between light and nonequilibrium carriers in 2D materials from these differential signals.

ACKNOWLEDGMENTS

Dr. Yan thanks Mr. Boye Sun for valuable discussions and revision. This work was supported by the Chinese National Key Basic Research Special Fund (2011CB922003), International Science and Technology Cooperation Program of China (2013DFA51430), NSFC—National Natural Science Foundation of China (11174159, 11374164, 11304166), and the Fundamental Research Funds for the Central Universities (65145005).

REFERENCES

1. S. F. Shi, T. T. Tang, B. Zeng, L. Ju, Q. Zhou, A. Zettl, and F. Wang, "Controlling graphene ultrafast hot carrier response from metal-like to semiconductor-like by electrostatic gating," Nano Lett. **14**, 1578–1582 (2014).
2. D. Brida, A. Tomadin, C. Manzoni, Y. J. Kim, A. Lombardo, S. Milana, R. R. Nair, K. S. Novoselov, A. C. Ferrari, G. Cerullo, and M. Polini, "Ultrafast collinear scattering and carrier multiplication in graphene," Nat. Commun. **4**, 1987 (2013).
3. M. Breusing, S. Kuehn, T. Winzer, E. Malic, F. Milde, N. Severin, J. P. Rabe, C. Ropers, A. Knorr, and T. Elsaesser, "Ultrafast nonequilibrium carrier dynamics in a single graphene layer," Phys. Rev. B **83**, 153410 (2011).
4. I. Gierz, J. C. Petersen, M. Mitrano, C. Cacho, I. C. E. Turcu, E. Springate, A. Stöhr, A. Köhler, U. Starke, and A. Cavalleri, "Snapshots of non-equilibrium Dirac carrier distributions in graphene," Nat. Mater. **12**, 1119–1124 (2013).
5. K. J. Tielrooij, J. C. W. Song, S. A. Jensen, A. Centeno, A. Pesquera, A. Zurutuza Elorza, M. Bonn, L. S. Levitov, and F. H. L. Koppens, "Photoexcitation cascade and multiple hot-carrier generation in graphene," Nat. Phys. **9**, 248–252 (2013).
6. A. Tomadin, D. Brida, G. Cerullo, A. C. Ferrari, and M. Polini, "Nonequilibrium dynamics of photoexcited electrons in graphene: collinear scattering, Auger processes, and the impact of screening," Phys. Rev. B **88**, 035430 (2013).
7. S. Ulstrup, J. C. Johannsen, F. Cilento, J. A. Miwa, A. Crepaldi, M. Zacchigna, C. Cacho, R. Chapman, E. Springate, S. Mammadov, F. Fromm, C. Raidel, T. Seyller, F. Parmigiani, M. Grioni, P. D. C. King, and P. Hofmann, "Ultrafast dynamics of massive Dirac fermions in bilayer graphene," Phys. Rev. Lett. **112**, 257401 (2014).
8. K. Chen, H. Li, L.-P. Ma, W. Ren, T.-F. Chung, H.-M. Cheng, Y. P. Chen, and T. Lai, "Diversity of ultrafast hot-carrier-induced dynamics and striking sub-femtosecond hot-carrier scattering times in graphene," Carbon **72**, 402–409 (2014).
9. K. Chen, H. Li, L.-P. Ma, W. Ren, J.-Y. Zhou, H.-M. Cheng, and T. Lai, "Ultrafast linear dichroism-like absorption dynamics in graphene grown by chemical vapor deposition," J. Appl. Phys. **115**, 203701 (2014).
10. B. Gao, G. Hartland, T. Fang, M. Kelly, D. Jena, H. L. Xing, and L. B. Huang, "Studies of intrinsic hot phonon dynamics in suspended graphene by transient absorption microscopy," Nano Lett. **11**, 3184–3189 (2011).
11. L. B. Huang, B. Gao, G. Hartland, M. Kelly, and H. L. Xing, "Ultrafast relaxation of hot optical phonons in monolayer and multilayer graphene on different substrates," Surf. Sci. **605**, 1657–1661 (2011).
12. M. M. Leandro, M. Kin Fai, A. H. C. Neto, N. M. R. Peres, and F. H. Tony, "Observation of intra- and inter-band transitions in the transient optical response of graphene," New J. Phys. **15**, 015009 (2013).
13. T. Li, L. Luo, M. Hupalo, J. Zhang, M. C. Tringides, J. Schmalian, and J. Wang, "Femtosecond population inversion and stimulated emission of dense Dirac fermions in graphene," Phys. Rev. Lett. **108**, 167401 (2012).
14. R. W. Newson, J. Dean, B. Schmidt, and H. M. van Driel, "Ultrafast carrier kinetics in exfoliated graphene and thin graphite films," Opt. Express **17**, 2326–2333 (2009).
15. B. A. Ruzicka, S. Wang, J. W. Liu, K. P. Loh, J. Z. Wu, and H. Zhao, "Spatially resolved pump-probe study of single-layer graphene produced by chemical vapor deposition [Invited]," Opt. Mater. Express **2**, 708–716 (2012).
16. J. Shang, S. Yan, C. Cong, H.-S. Tan, T. Yu, and G. G. Gurzadyan, "Probing near Dirac point electron–phonon interaction in graphene," Opt. Mater. Express **2**, 1713–1722 (2012).
17. J. Z. Shang, Z. Q. Luo, C. X. Cong, J. Y. Lin, T. Yu, and G. G. Gurzadyan, "Femtosecond UV-pump/visible-probe measurements of carrier dynamics in stacked graphene films," Appl. Phys. Lett. **97**, 163103 (2010).
18. J. Z. Shang, T. Yu, J. Y. Lin, and G. G. Gurzadyan, "Ultrafast electron-optical phonon scattering and quasiparticle lifetime in CVD-grown graphene," ACS Nano **5**, 3278–3283 (2011).
19. X.-Q. Yan, J. Yao, Z.-B. Liu, X. Zhao, X.-D. Chen, C. Gao, W. Xin, Y. Chen, and J.-G. Tian, "Evolution of anisotropic-to-isotropic photoexcited carrier distribution in graphene," Phys. Rev. B **90**, 134308 (2014).
20. F. Kadi, T. Winzer, E. Malic, A. Knorr, F. Göttfert, M. Mittendorff, S. Winnerl, and M. Helm, "Microscopic description of intraband absorption in graphene: the occurrence of transient negative differential transmission," Phys. Rev. Lett. **113**, 035502 (2014).
21. H. Yang, X. Feng, Q. Wang, H. Huang, W. Chen, A. T. S. Wee, and W. Ji, "Giant two-photon absorption in bilayer graphene," Nano Lett. **11**, 2622–2627 (2011).
22. H. Zhang, D. Tang, L. Zhao, Q. Bao, and K. Loh, "Large energy mode locking of an erbium-doped fiber laser with atomic layer graphene," Opt. Express **17**, 17630–17635 (2009).
23. B. Y. Sun and M. W. Wu, "Negative differential transmission in graphene," Phys. Rev. B **88**, 235422 (2013).
24. P. A. George, J. Strait, J. Dawlaty, S. Shivaraman, M. Chandrashekhar, F. Rana, and M. G. Spencer, "Ultrafast optical-pump terahertz-probe spectroscopy of the carrier relaxation and recombination dynamics in epitaxial graphene," Nano Lett. **8**, 4248–4251 (2008).
25. D. Svintsov, V. Ryzhii, A. Satou, T. Otsuji, and V. Vyurkov, "Carrier-carrier scattering and negative dynamic conductivity in pumped graphene," Opt. Express **22**, 19873–19886 (2014).
26. K. F. Mak, M. Y. Sfeir, Y. Wu, C. H. Lui, J. A. Misewich, and T. F. Heinz, "Measurement of the optical conductivity of graphene," Phys. Rev. Lett. **101**, 196405 (2008).
27. J. W. Weber, V. E. Calado, and M. C. M. van de Sanden, "Optical constants of graphene measured by spectroscopic ellipsometry," Appl. Phys. Lett. **97**, 091904 (2010).
28. X. Wang, M. Zhao, and D. D. Nolte, "Optical contrast and clarity of graphene on an arbitrary substrate," Appl. Phys. Lett. **95**, 081102 (2009).
29. M. Born and E. Wolf, *Principles of Optics* (Cambridge University, 1999).
30. M. Bruna and S. Borini, "Optical constants of graphene layers in the visible range," Appl. Phys. Lett. **94**, 031901 (2009).
31. F. J. Nelson, V. K. Kamineni, T. Zhang, E. S. Comfort, J. U. Lee, and A. C. Diebold, "Optical properties of large-area

polycrystalline chemical vapor deposited graphene by spectroscopic ellipsometry," Appl. Phys. Lett. **97**, 253110 (2010).
32. Q. Ye, J. Wang, Z. Liu, Z.-C. Deng, X.-T. Kong, F. Xing, X.-D. Chen, W.-Y. Zhou, C.-P. Zhang, and J.-G. Tian, "Polarization-dependent optical absorption of graphene under total internal reflection," Appl. Phys. Lett. **102**, 021912 (2013).
33. V. G. Kravets, A. N. Grigorenko, R. R. Nair, P. Blake, S. Anissimova, K. S. Novoselov, and A. K. Geim, "Spectroscopic ellipsometry of graphene and an exciton-shifted van Hove peak in absorption," Phys. Rev. B **81**, 155413 (2010).
34. "Fabry–Perot. interferometer," http://en.wikipedia.org/wiki/Fabry%E2%80%93P%C3%A9rot_interferometer.
35. "Coherence length," http://en.wikipedia.org/wiki/Coherence_length.
36. Q. Cui, F. Ceballos, N. Kumar, and H. Zhao, "Transient absorption microscopy of monolayer and bulk WSe2," ACS Nano **8**, 2970–2976 (2014).
37. N. Kumar, J. He, D. He, Y. Wang, and H. Zhao, "Valley and spin dynamics in MoSe2 two-dimensional crystals," Nanoscale **6**, 12690–12695 (2014).
38. R. Wang, B. A. Ruzicka, N. Kumar, M. Z. Bellus, H.-Y. Chiu, and H. Zhao, "Ultrafast and spatially resolved studies of charge carriers in atomically thin molybdenum disulfide," Phys. Rev. B **86**, 045406 (2012).